Shape Control of PbSe Nanocrystals Using Noble Metal Seed Particles

ARTICLE *in* NANO LETTERS · MAY 2006

Impact Factor: 13.59 · DOI: 10.1021/nl052472n · Source: PubMed

6 AUTHORS, INCLUDING:

Kaushik Roy Choudhury
Dupont
46 PUBLICATIONS **1,107** CITATIONS
SEE PROFILE

Mark Swihart
University at Buffalo, The State University of…
213 PUBLICATIONS **6,129** CITATIONS
SEE PROFILE

John Minter
Kodak
20 PUBLICATIONS **749** CITATIONS
SEE PROFILE

NANO LETTERS

2006
Vol. 6, No. 4
709−714

Shape Control of PbSe Nanocrystals Using Noble Metal Seed Particles

Ken-Tye Yong,[†,§] Yudhisthira Sahoo,[†,‡] Kaushik Roy Choudhury,[†,||] Mark T. Swihart,*[,†,§] John R. Minter,[⊥] and Paras N. Prasad*[,†,‡,||]

Institute for Lasers, Photonics and Biophotonics, Department of Chemistry, Department of Chemical and Biological Engineering, and Department of Physics, The University at Buffalo, The State University of New York, Buffalo, New York 14260-4200, and Foundation Science and Technology Center, Eastman Kodak Company, Research Laboratories, Rochester, New York 14650

Received December 14, 2005; Revised Manuscript Received February 15, 2006

ABSTRACT

We demonstrate that the shape of PbSe nanocrystals can be controlled systematically by seeding their growth with noble metal nanoparticles (Au, Ag, or Pd) and varying the seed and precursor concentrations. Cylinders (quantum rods), cubes, crosses, stars, and branched structures were produced in high yield at 150 °C in reaction times of a few minutes. Although their absorption spectrum does not exhibit sharp features, the quantum rods exhibit significant photogeneration efficiency, enabling infrared sensitization of a polymeric photoconductive nanocomposite.

The physical properties of semiconductor nanocrystals (NCs) are influenced strongly by their size and shape.[1−3] For the past two decades, a growing array of well-developed synthetic methodologies have been used to produce nearly monodispersed spherical NCs, also called quantum dots (QDs). The physical properties of the QDs were explored extensively with regard to the effect of quantum confinement on their optical and electronic properties. Recently, the effects of NC shape have received great attention because unique behavior is expected in the evolution from zero-dimensional (0D) QDs to one-dimensional (1D) quantum rods (QRs) or quantum wires (QWs).[4−6] For example, it was reported that CdSe QRs emitted light that was linearly polarized along the *c* axis of the crystallites and that the degree of polarization was dependent on the aspect ratio of the NCs.[5] It was also shown recently that magnetic QWs have higher blocking temperatures and magnetization than their QD counterparts. These early studies of anisotropic NCs show that nanostructures of different shapes (e.g., QRs and QWs) can offer new possibilities for tailoring material properties and offer improved performance when used as functional components in lasers or various other memory and optoelectronic devices.[7]

Several groups have reported shape-controlled synthesis of different colloidal NCs. Alivisatos' group[5,8−10] and Peng et al.[11−13] have developed a colloidal synthesis method for the formation of QRs and multipods of CdSe and CdTe. In their laboratories, the anisotropic nanostructures were synthesized via hot colloidal chemistry employing a binary mixture of surfactants that consisted of trioctylphosphine oxide (TOPO) and hexylphosphonic acid, whereby the growth of CdSe and CdTe NCs along the *c* axis was facilitated by preferential adsorption of phosphonic acid onto certain facets. Cheon et al.[14] showed that differences in the steric effects of surfactant ligands of the same kind (trioctylamine and hexadecylamine) could also be used to modulate the crystalline phases and control the shapes of NCs. Qian et al.[15] reported the formation of high aspect ratio PbS QRs at the interface of two immiscible solvents under biphasic solvothermal conditions. Lifshitz et al.[16] reported the use of various N-chelated molecules as solvent coordinating molecular templates that enabled the formation of PbSe nanostructures of various shapes. Another approach to anisotropic growth of such quantum structures is the solution−liquid−solid (SLS) method,[17] the solution counterpart of the vapor−liquid−solid (VLS) growth method that has been used to grow a variety of nanowires on solid substrates seeded with catalyst particles. This approach has been used to grow nanowires of a variety of materials.[17−25] SLS-grown InP and InAs QRs[26,27] have been reported recently by Banin et al. This method consists of seeding the colloidal reaction mixture with metal particles such as Au, Ag, or In NPs. Kuno et al.[18,20] synthesized straight and

* Corresponding authors. E-mail: swihart@eng.buffalo.edu; pnprasad@buffalo.edu.
[†] Institute for Lasers, Photonics and Biophotonics, The University at Buffalo.
[‡] Department of Chemistry, The University at Buffalo.
[§] Department of Chemical and Biological Engineering, The University at Buffalo.
[||] Department of Physics, The University at Buffalo.
[⊥] Foundation Science and Technology Center, Eastman Kodak Company.

10.1021/nl052472n CCC: $33.50
Published on Web 02/28/2006

branched CdSe and PbSe QWs by seeding with Au/Bi core/shell NPs. These synthetic methodologies have opened up new routes for preparing semiconductor NCs with tunable shape, size, and optical properties.

Among the IV−VI semiconductors, the PbSe NCs constitute an interesting system because of the ease of realizing quantum modulated optical behavior in the infrared (IR) range. Because of the large Bohr exciton radius in PbSe, about 46 nm, quantum confinement effects begin to appear at relatively large particle dimensions. Bulk PbSe has a rock salt crystal structure and is a direct gap semiconductor with a band gap of 0.28 eV. Solution processible PbSe NCs exhibit well-defined band-edge excitonic transitions tunable between 0.9 and 2.0 eV and small Stokes shifts.[2,28] They have been shown to be efficient photocharge generators at communication IR wavelengths.[29] Furthermore, they have been suggested as an effective system for deep tissue imaging.[30]

Here, we demonstrate the fabrication of PbSe NCs in a variety of shapes using noble metal nanoparticles (NPs) of Au, Ag, and Pd as seeds. The shape and size of the PbSe NCs depend strongly on the concentration and the type of the noble metal particles, and on the Pb-to-Se ratio in the growth solution. The Au, Ag, and Pd NPs, synthesized by the well-known two-phase method,[31−33] were obtained with average sizes of 4, 7, and 3 nm, respectively. In a typical experiment for the synthesis of anisotropic PbSe NCs, lead oxide (1 mmol), phenyl ether (3 mL), oleic acid (2 mL), and a known amount of gold, silver, or palladium NPs were mixed and heated to 150 °C for ∼35 min under an argon stream in a three-neck flask. The total amount of metal NPs used in this study was varied from ∼0.0005 to ∼0.0250 mmol of metal atoms. Following this, 1 mL of (TOP)Se solution (1 M Se in trioctylphosphine) was injected rapidly into the hot reaction mixture. A dark brown/black solution formed, which was kept at 150 °C briefly before being cooled gradually to room temperature. After synthesis, the PbSe NCs were precipitated by the addition of ethanol to the product mixture followed by centrifugation. The details of the preparation procedure can be found in the Supporting Information. A summary of reaction conditions used for different shapes and sizes of PbSe NCs is presented there in Table S1.

It is clear from these experiments that the most important parameter in determining the shape, size, and structure of PbSe NCs is the concentration of the metal NPs, followed by the Pb:Se precursor ratio. The dimensions and structure of the PbSe NCs change significantly as the metal concentration is changed. In the absence of any metal seed particles, slightly anisotropic ovoid or diamond-shaped nanocrystals were formed, with an aspect ratio of about 1.5 (see Figure S1 in the Supporting Information). At low concentration of gold NPs (∼0.0005 mmol metal atoms and a Pb:Se ratio of 1:1), QRs and T-shaped and L-shaped particles were formed, with QRs constituting the vast majority (>90%) as shown in Figure 1a. As shown in Figure 2a, at an early stage (i.e., within the first 30 to 45 s) of the reaction, the rod length was relatively small, but it increased progressively with the

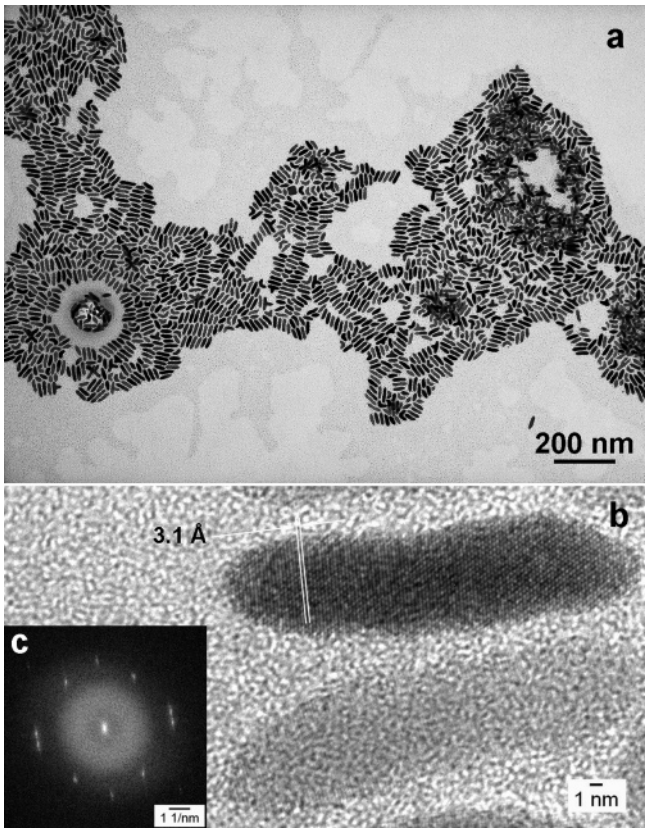

Figure 1. (a) TEM image of PbSe QRs showing that they are highly monodisperse and that more than 90% of particles are rods. The average length and width of the QRs are 38.7 and 10.3 nm, respectively. (b) HRTEM image of PbSe QRs with lattice fringes of 3.1 Å. (c) Corresponding FFT image from the rod shown in part b.

growth time (see Figure 2b and c). However, the aspect ratio of the rods remained roughly constant. When the gold NP concentration was increased to ∼0.005 mmol metal atoms, no PbSe QRs were formed; instead, cross-shaped PbSe NCs appeared (Figure 2d). Upon further increase in the gold NP concentration to ∼0.0250 mmol metal atoms, gold core−PbSe shell structures appeared (Figure 2e). High-resolution TEM (HRTEM) and selected area electron diffraction (SAED) clearly showed the presence of both Au and PbSe in these nanoparticles and confirmed the core−shell structure (see Supporting Information, Figures S2 and S3). T-, cube-, and dot-shaped particles were formed, respectively (Figure 2f, g, and h), by changing the Pb:Se ratio from 1:1 to 2:1, 3:1 or 1:2, while maintaining the gold NP concentration at ∼0.0005 mmol metal atoms.

The XRD pattern of PbSe crystalline QRs is shown in Figure 3. All of the diffraction peaks correspond to the cubic rock-salt structure of PbSe. The (200) peak is less broadened than the others, indicating a longer-range order in that direction, which corresponds to the axis of the QRs. No discernible peaks of Au were observed, apparently because of the very small amount of Au used. The lattice fringes of the PbSe QRs are shown clearly in Figure 1b, with fringe spacing of 3.1 Å. These fringes, which correspond to (200) lattice planes for the cubic rock salt structure of PbSe, are aligned perpendicular to the rod axis. This confirms that the

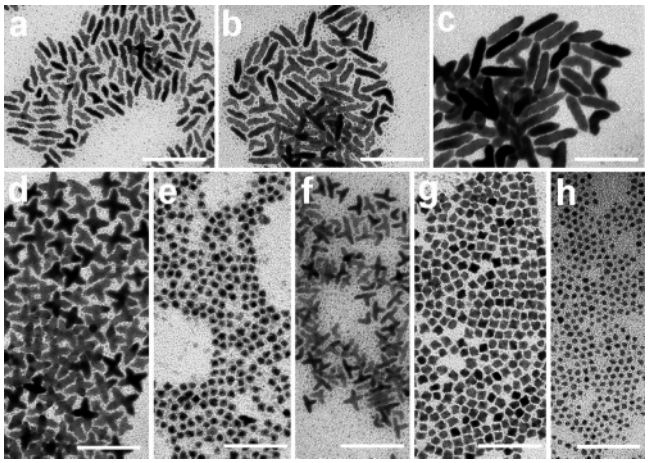

Figure 2. TEM images of PbSe nanocrystals synthesized with Au NPs under different conditions. (a−c) PbSe QRs synthesized with ∼0.0005 mmol of Au NPs. The growth time increases from a to c (see the Supporting Information). (d) Cross-shaped PbSe NCs synthesized with ∼0.005 mmol Au NPs. (e) Au/PbSe core/shell structure synthesized with ∼0.025 mmol Au NPs. (f) T-shaped PbSe nanocrystals obtained at Pb:Se ratio of 1:2 with ∼0.0005 mmol of Au NPs. (g) Cubelike PbSe nanocrystals synthesized at Pb:Se ratio of 2:1 with ∼0.0005 mmol of Au NPs. (h) PbSe QDs synthesized at Pb:Se ratio of 3:1 with ∼0.0005 mmol of Au NPs. The scale bars are 70 nm.

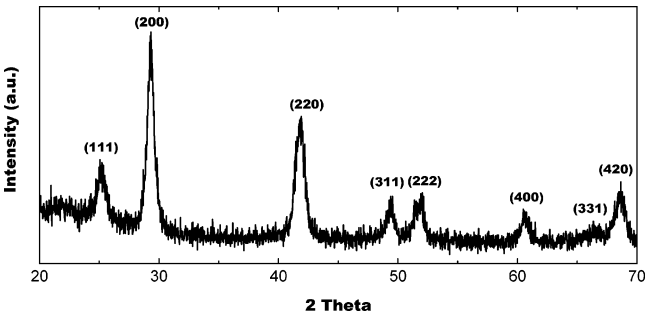

Figure 3. XRD pattern of PbSe QRs like those shown in Figure 1.

QRs elongation axis was in the [100] direction. Both the XRD and the HRTEM results confirm that the long axis of the QRs corresponds to the [100] direction of the cubic rock salt structure.

A high yield (approximately 90% of the nanocrystal population) of diamond-shaped PbSe NCs was obtained by using silver NPs at low concentration (∼0.0005 mmol metal atoms); see Figure 4a. When the reaction was performed at a higher concentration of Ag NPs (∼0.025 mmol metal atoms), multibranched crystals were formed (Figure 4b−e). Notably, no free-standing discrete rods were observed, in contrast to the synthesis using the same concentration of Au NPs. Note that because the silver NPs are larger than the gold ones used here, an equal metal atom concentration corresponds to a seed particle number concentration that is about a factor of 5 smaller for silver than for gold. At this very low seed particle concentration, there may be a significant number of "unseeeded" PbSe nanocrystals formed, and indeed some of the particles observed here are similar to those observed in the absence of metal seeds. However,

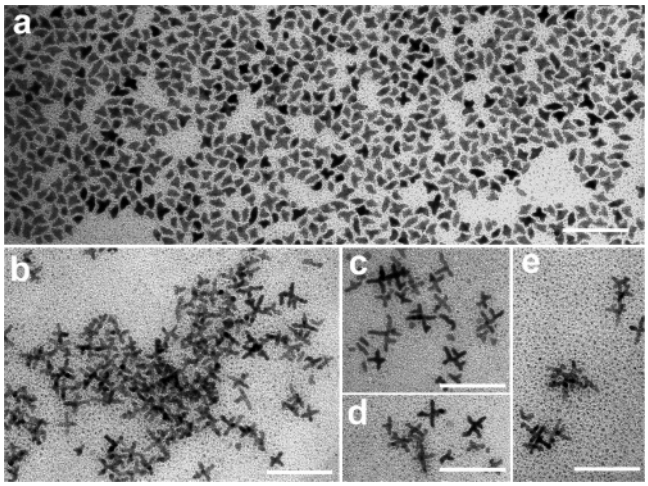

Figure 4. TEM images of PbSe nanocrystals synthesized with Ag NPs under different conditions. (a) Diamond-like PbSe NCs synthesized with ∼0.0005 mmol of Ag NPs. (b−e) Multibranch-shaped PbSe NCs synthesized with ∼0.025 mmol Ag NPs. The scale bars are 70 nm.

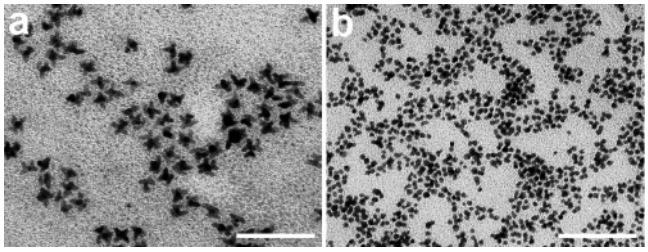

Figure 5. TEM images of PbSe nanocrystals synthesized with Pd NPs. (a) Starlike PbSe NCs synthesized with ∼0.0005 mmol of Pd NPs. (b) Quasi-spherical PbSe NCs synthesized with ∼0.025 mmol. The scale bars are 70 nm.

there is still an obvious effect of the metal NPs on the morphology of most of the NCs.

When Pd NPs were used as the seeds at a level of ∼0.0005 mmol metal atoms, star-shaped PbSe NCs were formed (Figure 5a). The yield of the star-shaped particles was as high as ∼90% of the NC population. Quasi-spherical PbSe NCs were obtained by further increasing the concentration to ∼0.025 mmol (Figure 5b).

Figure 6 shows HRTEM images of highly crystalline T-shaped, multibranched, diamond-shaped, and star-shaped PbSe NCs. These also show lattice fringes of the cubic PbSe lattice. The T-shaped, multibranched, and diamond-shaped PbSe NCs have fringe spacing of 3.1 Å, which corresponds to (200) lattice planes for the cubic rock salt structure of PbSe. However, the star-shaped PbSe NCs have fringe spacing of 3.6 Å, corresponding to the PbSe(111) planes. For the branched structures shown in parts a−c of Figure 6, two perpendicular sets of (200) planes are visible, as also reflected in the Fourier transforms of these images. As for the unbranched (simple) rods, the growth direction for each branch of these is the [100] direction. This constrains the branches to be at ∼90 degree angles from each other. It appears from the HRTEM that the PbSe QRs synthesized in this work are solid rods and are not a fused string of individual PbSe NCs as reported by Cho et al.[34] Additionally,

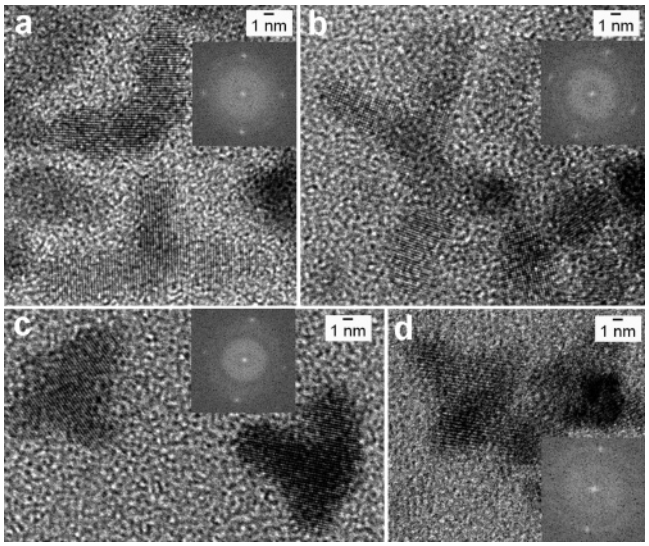

Figure 6. HRTEM images of different PbSe nanocrystals synthesized with Au, Ag, and Pd NPs. (a) L- and T-shaped PbSe NCs corresponding to Figure 2f. (b) Multibranched PbSe NCs corresponding to Figure 4b−e. (c) Diamond-shaped PbSe NCs corresponding to Figure 4a. (d) Star-shaped PbSe NCs corresponding to Figure 5a. Insets give the Fourier transforms of (a) the NC just to the left of the inset, (b) the upper-left portion of the branched NC to the left of the inset, (c) the NC just below the inset, and (d) the NC in the upper left.

we note that the width of PbSe QRs shown in Figure 1 is smaller than the Bohr exciton radius in PbSe (46 nm). The electrons and holes in the QRs should be strongly quantum confined.

The formation of various shapes of PbSe NCs must result from changes in the PbSe nanocrystal nucleation and growth kinetics in the presence of the metallic NPs. Most previous studies of metal-seeded solution-phase growth of crystalline semiconductor nanowires and nanorods have been interpreted in terms of the solution−liquid−solid (SLS) mechanism proposed by Trentler et al.[17] In the present experiments, however, the metallic seed particles are probably not molten under the growth conditions. Even accounting for the size-reduction of the melting point,[35] temperatures above 700 °C are required to melt 4 nm gold particles such as those used as seeds here. The Au−Pb phase diagram[36] shows that lower melting point solutions can form, down to the $AuPb_3$ − Pb eutectic temperature of 215 °C, but this requires the formation of metallic lead and intermetallic compounds. In control experiments in which the selenium precursor was omitted, no metallic lead or Au−Pb intermetallic compounds formed. Thus, it is most likely that the PbSe growth is catalyzed not by a liquid metal droplet but by a metal nanocrystal. The seed nanocrystal may have a quasi-molten surface layer, as has been predicted by some molecular dynamics simulations of metal nanocrystal melting.[37−39] Solid-state diffusion of Pb or Se within the metal seed particles is also unlikely because the solubility of both Pb and Se in the noble metals is very small (at least in the bulk).[36] Thus, we expect that the essential contribution of the seed particle is simply to provide a low-energy interface for heterogeneous nucleation of the PbSe nanocrystal. We hypothesize that, initially, one or more PbSe rods nucleate on each seed particle and that when the rod length exceeds a critical value it detaches from the nucleation site. This would be expected to occur when the total internal crystal strain energy, due to lattice mismatch between the metal and PbSe, becomes sufficiently large, as the length of the rod increases. We speculate that the mechanism of formation of branched structures may be similar to the geminate nanowire nucleation mechanism proposed by Kuno and co-workers.[18,20] If multiple rods are growing simultaneously from a single seed crystal, then they may merge to produce branched structures, prior to being cleaved from the seed nanocrystal.

In support of the claim that multiple rods are seeded by each noble metal particle, we estimate the ratio of the number of rods produced to the number of seed particles as follows. A 4-nm-diameter Au sphere has a volume of $\sim 3.4 \times 10^{-20}$ cm^3, a mass of $\sim 6.5 \times 10^{-19}$ g, and contains ~2000 atoms. For nanorod synthesis, the total amount of gold used was $\sim 5 \times 10^{-7}$ mol, corresponding to $\sim 1.5 \times 10^{14}$ Au nanoparticles. Comparing this to the 1 mmol of Pb and Se precursors used, we have about 4×10^6 precursor molecules per seed particle. We determined the yield of particles gravimetrically in an experiment that produced rods with an average diameter of 8.5 nm and average length of 32.5 nm, as determined from manual counting and measurement of TEM images. The mass of recovered particles, after three cycles of washing with ethanol, precipitation, and centrifugation, was 18.2 mg. Thermogravimetric analysis showed an additional 35% weight loss, assignable to the organic surfactant components. Thus, a final yield of ~11.8 mg of product was obtained. This corresponds to ~4% of the maximum theoretical yield of 286.2 mg from 1 mmol of each precursor, but the actual yield may have been significantly higher because losses are likely during the multiple washing steps. A PbSe rod 8.5 nm in diameter by 32.5 nm long has a volume of $\sim 1.8 \times 10^{-18}$ cm^3, a mass of $\sim 1.5 \times 10^{-17}$ g, and contains ~32 000 atoms each of Pb and Se. If each nanoparticle generated only a single rod of this size, then the yield of PbSe would be only about 32 000/4 000 000 = 0.8%. This is a factor of 5 smaller than the measured lower limit of the PbSe yield. Therefore, on average, several rods must be produced per seed particle. This, in turn, requires that the rods cleave from the seed particles because individual rods are observed in the final products.

The estimates in the preceding paragraph suggest that for conditions that result in the formation of simple (unbranched) rods, the precursors are not significantly depleted in the reaction times used here (up to ~4 min). From the results shown in parts a−c of Figure 2, it also appears that the rods continue to grow anisotropically after cleaving from the seed particles. For that experiment, the aspect ratio of the rods remained nearly constant as the rods roughly doubled in both length and diameter and maintained their simple rod morphology. Significantly longer reaction times led to precipitation of large agglomerates, which also supports the suggestion that substantial precursor remains in the reactor after these short reaction times. For higher seed particle concentrations, substantial precursor depletion may have occurred.

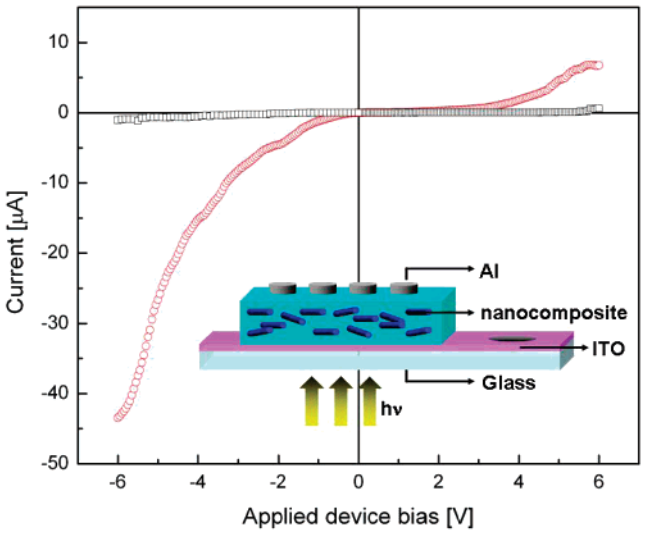

Figure 7. Photocurrent (circles) and dark current (squares) as a function of applied voltage in a PbSe nanorods/PVK composite device at the infrared wavelength of 1.34 μm. The inset shows a schematic of the sandwich nanocomposite device structure.

Because the local concentration of precursor around each seed particle is, initially, independent of the total number of seed particles, one would expect the initial nucleation to be independent of the seed particle concentration. However, when the seed particle concentration is increased by an order of magnitude from that used in the estimates above, then the same number of nucleation sites per particle would lead to substantial precursor depletion. This, in turn, would slow the growth rate, allowing more time for the rods growing from a given seed to align and fuse together, producing T- or cross-shaped particles such as those shown in Figure 2d. Further increases in the seed particle concentration could result in complete depletion of precursors prior to cleavage of the rods from the seed particles. This would lead to core−shell particles with rough, polycrystalline shells (resulting from multiple nucleation sites) like those shown in Figure 2e and Figure S2. Similarly, differences in nucleation and growth kinetics on the different metals used as seeds and for different precursor ratios could account for the varying propensity for the formation of branched versus simple rods, in the context of competition between growth to the point where the nanocrystal cleaves from the seed versus alignment and merger of multiple rods growing from a single seed.

To demonstrate an application of these nanostructures in optoelectronic devices, we fabricated composite photodetectors containing the PbSe QRs (length: 21 nm, diameter: 5.5 nm) and a photoconductive polymer, poly-*N*-vinylcarbazole (PVK), as shown schematically in the inset of Figure 7. Previous studies have shown that PbSe quantum dots (QDs) incorporated into such polymeric composites can provide efficient photodetection at IR wavelengths.[29] Despite the lack of any distinct maximum in the absorption spectrum of the QR's, which might be due to the convolution of absorption peaks at several wavelengths from rods of different dimensions, the nanorods photosensitize the polymer successfully at an IR wavelength. Figure 7 shows the current−voltage ($I-V$) behavior of this device in the presence and absence of 1.34 μm infrared light. Both $I-V$ curves show nonlinear behavior, with the photocurrent more than an order of magnitude larger than the dark current. The photocurrent response corresponds to a photogeneration quantum efficiency of ∼0.25% at the highest operational bias for ∼200-nm-thick samples. Judicious tailoring of the NC dimensions and optimized device compositions are expected to enhance the photogeneration efficiency at the desired operating wavelength, leading to much better photoconductive performance.

In summary, a facile hot colloidal metallic seed-mediated method was developed, which provides control of the shape, size, and structure of PbSe NCs by manipulating the type of noble metal NPs and synthesis parameters. Nanocrystals of various shapes, including cylinders, cubes, crosses, stars, and branched structures were produced in high yield at 150 °C within the first few minutes after the start of the synthesis. The optical absorption and luminescence of these multipod structures are similar to those of the corresponding quantum dots, though with a lower quantum efficiency as expected because of reduced quantum-confinement effects. Preliminary studies indicate that the NCs can be integrated successfully into solution-processed, high-performance, large-area photoconductive devices.

Acknowledgment. This work was supported in part by a Defense University Research Initiative on Nanotechnology grant, through the Chemistry and Life Sciences Directorate of the Air Force Office of Scientific Research.

Supporting Information Available: Detailed materials and methods; TEM image of particles prepared without metal seeds; HRTEM image of core−shell nanoparticles; selected area electron diffraction pattern from core−shell nanoparticles; HRTEM image of PbSe quantum dots; table with details of experimental conditions and resulting particle morphologies. This material is available free of charge via the Internet at http://pubs.acs.org.

References

(1) Prasad, P. N. *Nanophotonics*; Wiley-Interscience: New York, 2004.
(2) Du, H.; Chen, C.; Krishnan, R.; Krauss, T. D.; Harbold, J. M.; Wise, F. W.; Thomas, M. G.; Silcox, J. *Nano Lett.* **2002**, *2*, 1321−1324.
(3) Pietryga, J. M.; Schaller, R. D.; Werder, D.; Stewart, M. H.; Klimov, V. I.; Hollingsworth, J. A. *J. Am. Chem. Soc.* **2004**, *126*, 11752−11753.
(4) Kudera, S. C.; Carbone, L.; Casula, M. F.; Cingolani, R.; Falqui, A.; Snoeck, E.; Parak, W. J.; Manna, L. *Nano Lett.* **2005**, *5*, 445−449.
(5) Peng, X.; Manna, L.; Yang, W.; Wickham, J.; Scher, E.; Kadavanich, A.; Alivisatos, A. P. *Nature* **2000**, *404*, 59−61.
(6) Burda, C.; Chen, X.; Narayanan, R.; El-Sayed, M. A. *Chem. Rev.* **2005**, *105*, 1025−1102.
(7) Huynh, W. U.; Dittmer, J. J.; Alivisatos, A. P. *Science* **2002**, *295*, 2425−2427.
(8) Manna, L.; Scher, E. C.; Alivisatos, A. P. *J. Am. Chem. Soc.* **2000**, *122*, 12700−12706.
(9) Manna, L.; Scher, E. C.; Li, L.-S.; Alivisatos, A. P. *J. Am. Chem. Soc.* **2002**, *124*, 7136−7145.
(10) Manna, L.; Milliron, D.; Meisel, A.; Scher, E.; Alivisatos, A. P. *Nat. Mater.* **2003**, *2*, 382−385.
(11) Peng, Z. A.; Peng, X. *J. Am. Chem. Soc.* **2001**, *123*, 183−184.
(12) Peng, Z. A.; Peng, X. *J. Am. Chem. Soc.* **2001**, *123*, 1389−1395.
(13) Peng, Z. A.; Peng, X. *J. Am. Chem. Soc.* **2002**, *124*, 3343−3353.

(14) Kim, Y. H.; Jun, Y.-W.; Jun, B. H.; Lee, S.-M.; Cheon, J. *J Am. Chem. Soc.* **2002**, *124*, 13656−13657.
(15) Mo, M.-S.; Shao, M.-W.; Hu, H.-M.; Yang, L.; Yu, W.-C.; Qian, Y.-T. *J. Cryst. Growth* **2002**, *244*, 364−368.
(16) Lifshitz, E.; Bashouti, M.; Kloper, V.; Kigel, A.; Eisen, M. S.; Berger, S. *Nano Lett.* **2003**, *3*, 857−862.
(17) Trentler, T. J.; Hickman, K. M.; Goel, S. C.; Viano, A. M.; Gibbons, P. C.; Buhro, W. E. *Science* **1995**, *270*, 1791−1794.
(18) Hull, K. L.; Grebinski, J. W.; Kosel, T. H.; Kuno, M. *Chem. Mater.* **2005**, *17*, 4416−4425.
(19) Holmes, J. D.; Johnston, K. P.; Doty, R. C.; Korgel, B. A. *Science* **2000**, *287*, 1471−1473.
(20) Grebinski, J. W.; Hull, K. L.; Zhang, J.; Kosel, T. H.; Kuno, M. *Chem. Mater.* **2004**, *16*, 5260−5272.
(21) Hanrath, T.; Korgel, B. A. *J. Am. Chem. Soc.* **2002**, *124*, 1424−1429.
(22) Trentler, T. J.; Goel, S. C.; Hickman, K. M.; Viano, A. M.; Chiang, M. Y.; Beatty, A. M.; Gibbons, P. C.; Buhro, W. E. *J. Am. Chem. Soc.* **1997**, *119*, 2172−2181.
(23) Yu, H.; Buhro, W. E. *Adv. Mater.* **2003**, *15*, 416−419.
(24) Yu, H.; Li, J. B.; Loomis, R. A.; Wang, L. W.; Buhro, W. E. *Nat. Mater.* **2003**, *2*, 517−520.
(25) Yu, H.; Li, J. B.; Loomis, R. A.; Gibbons, P. C.; Wang, L. W.; Buhro, W. E. *J. Am. Chem. Soc.* **2003**, *125*, 16168−16169.
(26) Kan, S.-H.; Mokari, T.; Rothenberg, E.; Banin, U. *Nat. Mater.* **2003**, *2*, 155−158.
(27) Kan, S.-H.; Aharoni, A.; Mokari, T.; Banin, U. *Faraday Discuss.* **2004**, *125*, 23−38.
(28) Wehrenberg, B. L.; Wang, C.; Guyot-Sionnest, P. *J. Phys. Chem. B.* **2002**, *106*, 10634−10640.
(29) Roy Choudhury, K.; Sahoo, Y.; Ohulchanskyy, T. Y.; Prasad, P. N. *Appl. Phys. Lett.* **2005**, *87*, 073110.
(30) Lim, Y. T.; Kim, S.; Nakayama, A.; Stott, N. E.; Bawendi, M. G.; Frangioni, J. V. *Mol. Imaging* **2003**, *2*, 50−64.
(31) Brust, M.; Walker, M.; Bethell, D.; Schiffrin, D. J.; Whyman, R. *J. Chem. Soc., Chem. Commun.* **1994**, 802−803.
(32) Leff, D. V.; Ohara, P. C.; Heath, J. R.; Gelbart, W. M. *J. Phys. Chem.* **1995**, *99*, 7036−7041.
(33) Leff, D. V.; Brandt, L.; Heath, J. R. *Langmuir* **1996**, *12*, 4723−4730.
(34) Cho, K.-S.; Talapin, D. V.; Gaschler, W.; Murray, C. B. *J. Am. Chem. Soc.* **2005**, *127*, 7140−7147.
(35) Dick, K.; Dhanasekaran, T.; Zhang, Z. Y.; Meisel, D. *J. Am. Chem. Soc.* **2002**, *124*, 2312−2317.
(36) *Smithells Metals Reference Book*, 7th ed.; Brandes, E. A., Brook, G. B., Eds.; Butterworth-Heinemann: Boston, MA, 1998.
(37) Cleveland, C. L.; Luedtke, W. D.; Landman, U. *Phys. Rev. B* **1999**, *60*, 5065−5077.
(38) Cleveland, C. L.; Luedtke, W. D.; Landman, U. *Phys. Rev. Lett.* **1998**, *81*, 2036−2039.
(39) Miao, L.; Bhethanabotla, V. R.; Joseph, B. *Phys. Rev. B* **2005**, *72*, 134109.

NL052472N